Available online at www.sciencedirect.com
ScienceDirect
Journal of the Mechanics and Physics of Solids 56 (2008) 2473–2493
JOURNAL OF THE MECHANICS AND PHYSICS OF SOLIDS
www.elsevier.com/locate/jmps

Continuum characterization of novel pseudoelasticity of ZnO nanowires

A.J. Kulkarni, M. Zhou*

The George W. Woodruff School of Mechanical Engineering, Georgia Institute of Technology, Atlanta, GA 30332-0405, USA

Received 23 October 2007; received in revised form 20 January 2008; accepted 24 February 2008

Abstract

A novel pseudoelastic behavior was recently discovered in [0 1 $\bar{1}$ 0]-oriented ZnO nanowires under uniaxial tensile loading and unloading. This behavior results from a reversible transformation from the parent wurtzite (WZ) structure to a previously unknown graphitic structure (HX) and is associated with recoverable strains up to 16%. In this paper, a micromechanical continuum model is developed to characterize this behavior. Using the first law of thermodynamics, the model decomposes the transformation into an elastic process of structural transitions between WZ and HX through a sequence of thermodynamically reversible phase equilibrium states and a thermodynamically irreversible process of interface propagation. The elastic equilibrium transition process is modeled with strain energy functions of the two constituent phases which are obtained from independent molecular dynamics calculations. The dissipative interface propagation process is modeled phenomenologically with a function which relates dissipation to the interfacial area between the two phases. The model captures major characteristics of the behavior of wires with lateral dimensions between 20 and 40 Å over the temperature range of 100–500 K.

Keywords: Micromechanical model; Zinc oxide; Nanowires; Pseudoelasticity; Phase transformation

1. Introduction

Tetrahedrally bonded semiconductors such as ZnO, GaN, and SiC with a degree of covalency are normally brittle with fracture strains of at most 0.01–0.03% at the macroscale. However, as the characteristic size scale of the materials decreases to submicrons or nanometers, as in slender 1D structures such as nanowires and nanorods, a transition from the normally brittle behavior with small failure strains to a pseudoelastic response is observed (Kulkarni et al., 2006, 2007). Underlying this transition are novel kinematically reversible phase transformations previously unknown in bulk materials. For example, ZnO nanowires with the [0 1 $\bar{1}$ 0] growth orientation were recently found to exhibit a pseudoelastic behavior with recoverable strains up to 16%. This behavior results from a phase transformation from wurtzite (WZ) to a graphitic phase (HX) (Kulkarni et al., 2007). Similarly, ZnO nanowires with the [0 0 0 1] growth orientation can undergo another phase

*Corresponding author. Tel.: +1 404 894 3294; fax: +1 404 894 0186.
E-mail address: min.zhou@gatech.edu (M. Zhou).

0022-5096/$ - see front matter © 2008 Published by Elsevier Ltd.
doi:10.1016/j.jmps.2008.02.005

transformation from wurtzite to a previously unknown body-centered-tetragonal phase (BCT-4) and deform to strains up to 17% (Wang et al., 2007b). These phenomena are unique to the nanoscale and are not observed in bulk ZnO. The reversibility of the transformations endows the nanowires with large recoverable strains. The nearly defect-free nature of these nanowires and their large surface-to-volume ratios give rise to high atomic mobility and the ability to undergo significant deformations discussed here without fracture.

It is worth noting that the above phenomena echo similar discoveries in other slender 1D nanomaterials. Experiments revealed that Au nanowires can be pseudoelastic (Landman et al., 1996). Recently, single crystalline nanowires of Cu, Au, and Ni were shown to possess a novel shape memory effect (SME) and an underlying pseudoelasticity which do not exist in bulk (Liang and Zhou, 2005, 2006; Liang et al., 2005; Park et al., 2005). Pseudoelasticity with recoverable strains up to 15% has also been observed in carbon nanotubes (Yakobson et al., 1996). These pseudoelastic behaviors are similar in phenomenology. The responsible lattice level deformation mechanisms, however, can be different for different materials. For example, in the metal nanowires lattice reorientation within the FCC crystalline structure and a twin boundary propagation process are responsible. The driving force is the difference in surface energy and the anisotropic elastic response of the FCC lattice in the [1 1 0] and [0 0 1] directions. In [0 1 $\bar{1}$ 0]-oriented ZnO nanowires, the driving force is primarily due to the difference in chemical free energies between the WZ and HX crystalline structures, although surface energy difference between the WZ and HX wire configurations also plays a role. In both cases, an energy barrier exists between the parent (initial) and target (transformed) configurations. Also, clear size and temperature dependence of behavior exists in both cases because of surfaces. In this paper, our interest is on ZnO nanowires with the [0 1 $\bar{1}$ 0] axial orientation. The objectives are (1) to develop a constitutive model that captures both the pseudoelastic behavior and the intrinsic dependence of the behavior on size and temperature, (2) to provide a quantification of the behavior through the model, (3) to use this model to delineate and analyze the reversible (elastic WZ$\leftrightarrow$HX transformation) and irreversible (dissipative interface propagation) processes responsible for the novel pseudoelastic behavior at the nanoscale, and (4) to quantify the contributions of constituent elasticity, interface energy, and dissipation to the overall constitutive behavior of the nanowires.

Fig. 1(a) illustrates the WZ and HX crystalline structures involved in the transformation of [0 1 $\bar{1}$ 0]-oriented ZnO nanowires (Kulkarni et al., 2006). The corresponding response of a nanowire with a 40.81 Å $\times$ 39.89 Å cross-section at 100 K obtained from molecular dynamics (MD) simulations is shown in Fig. 1(b). The pseudoelastic response can be considered as consisting of the following eight stages outlined schematically in Fig. 1(c):

(1) A$\rightarrow$B: elastic deformation of the WZ-structured wire;
(2) B$\rightarrow$C: initiation of the WZ-to-HX phase transformation entailing a precipitous drop in stress;
(3) C$\rightarrow$D: propagation of the phase boundary from HX regions into WZ regions, with point D corresponding to the completion of the transformation;
(4) D$\rightarrow$E: elastic deformation of the HX-structured wire;
(5) E$\rightarrow$F: elastic unloading of the HX-structured wire, which continues beyond the point of initial transformation completion (D).
(6) F$\rightarrow$G: initiation of the reverse (HX-to-WZ) transformation with an increase in stress;
(7) G$\rightarrow$H: progression of the reverse transformation through the propagation of the phase boundary from WZ regions into HX regions, culminating in the reversion of the entire wire back to the WZ structure at point H;
(8) H$\rightarrow$A: elastic unloading of the WZ-structured wire.

The response, including the elastic deformations of the two phases and a contribution from the transformation, illustrates the nanowires' ability to undergo large deformations with recoverable strains up to 16% (Kulkarni et al., 2007). This is quite extraordinary since ionic compound semiconductors such as ZnO, GaN, InN, and BN are normally brittle. Such large recoverable strains and property variations associated with the transformation make these nanowires ideal candidates for nanocomponents in a variety of nano-electro-mechanical systems (NEMS), such as sensors, actuators, and switches. Since this novel response has

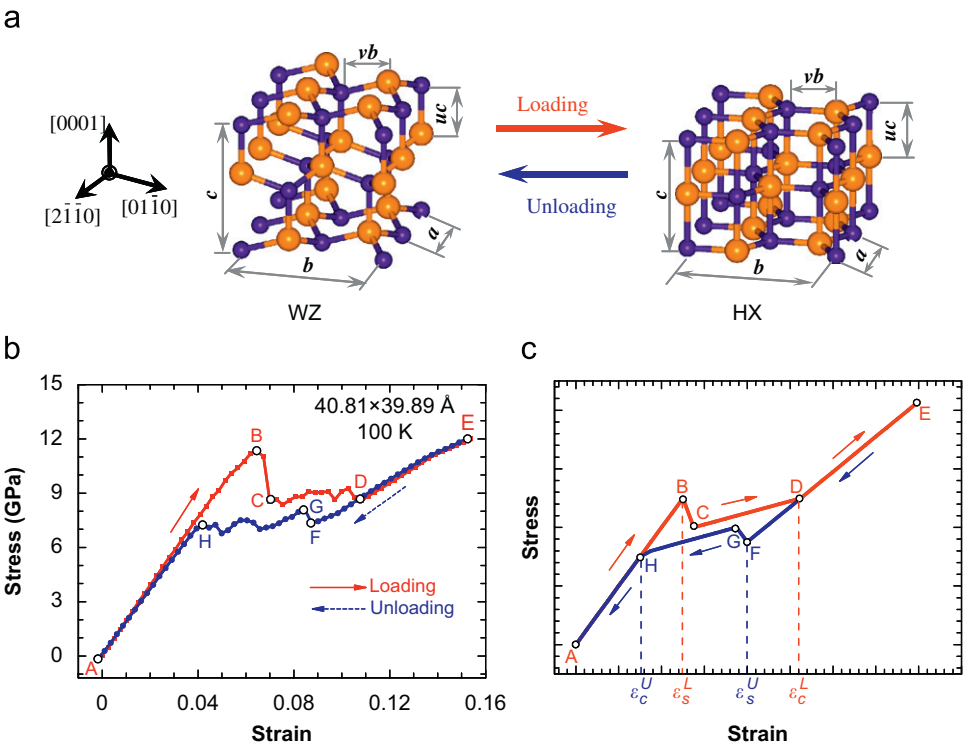

Fig. 1. (a) Crystalline structures of the parent WZ and transformed HX phases, (b) the response of a [0 1 $\bar{1}$ 0]-oriented nanowire under quasistatic tensile loading and unloading as obtained by MD simulation, and (c) a schematic illustration of the stages of deformation in (b).

only been discovered recently, the overall constitutive behavior including the driving force for the transformation, energy barriers for phase nucleation and the effects of size and temperature has not been quantified and analytically described.

In what follows next, a constitutive model for this pseudoelastic behavior accounting for all the deformation stages outlined above is developed. The micromechanical approach of Liang et al. (2007) originally used to model the pseudoelastic behavior of shape memory FCC metal nanowires is adopted. This framework focuses on the thermodynamic relations among the internal energies of the phases, dissipation and external work during loading and unloading. The total energy of a nanowire is expressed as the sum of the internal energies of the pure phases and the energy of the interface between the phases. This expression allows the elastic deformations before and after the forward and reverse transformations (A→B, D→E, E→F, and H→A) and the elastic (equilibrium) part of the transformation processes (B→C→D and F→G→H) to be characterized. The internal energies of the WZ and HX phases are obtained from MD calculations. The energy of the interface is quantified phenomenologically as a function of the total interfacial area which in turn is assumed to be a function of the volume fractions of the WZ and HX phases. Within this framework, the total energy depends on three independent variables which are the strain in the WZ phase relative to its equilibrium state (ε_1), the strain in the HX phase relative to its own equilibrium state (ε_2), and the volume fraction of the HX phase (f). At any given level of the overall deformation of a wire, these microscopic independent variables are determined by the requirement that the total energy of the wire is minimized. Similar to the strain energy of the interface, the dissipative part of the transformation process associated with the propagation of the interface is also accounted for phenomenologically, through a functional form involving the volume fraction of the HX phase as the independent state variable. The underlying assumption is that energy dissipation associated with the propagation of the interface between the HX and WZ phases is proportional to the total interface area. Overall, the first law of thermodynamics allows the external stress required to effect the deformation of the wire to be obtained as the sum of the stress associated with the elastic process of

equilibrium transition and the stress required to drive the dissipative propagation of the interface between the WZ and HX phases.

2. Background

Micromechanical models which couple micromechanics and thermodynamics principles have traditionally been used to describe the constitutive behaviors of shape memory alloys or SMAs (Muller and Xu, 1991). Such models are based on the existence of a non-convex free energy function which reflects the possibility of phase transformations (Huo and Muller, 2003). This framework has been successfully used to study martensitic transformations in SMAs whose strain energy functions have multiple local minima (Abeyratne and Knowles, 1993; Abeyratne and Kim, 1994; Abeyratne and Bhattacharya, 2001). However, kinetic laws (which are required in fully dynamic analyses) that relate driving force and interface motion which dictate dissipation are extremely difficult to obtain and pose a practical obstacle to the use of such models. Alternatively, the behavior can be modeled by decomposing the response into a process of transitions between static equilibrium states and a process of interface propagation, such that the overall dissipation is captured phenomenologically in an averaged sense and the details of the kinetic processes are not resolved. Liang et al. (2007) successfully applied this approach to the modeling of the pseudoelastic behavior of FCC metal nanowires. Since the transformation process during loading modeled thereof occurs through the propagation of a single twin boundary, the structure and size of the interface between the phases remain constant. Consequently, the interfacial energy remains constant and therefore does not contribute to the overall stress. However, in general, both the structure and size of the interference between the parent and target phases change during the transformation (Huo and Muller, 2003), as is the case of the ZnO nanowires analyzed here or even during unloading of the FCC nanowires analyzed by Liang et al. (2007). In such cases, the evolution of interfacial energy has to be explicitly considered. The approach developed by Muller and Xu (1991) considers the interface as one continuous surface with a certain amount of interface energy. A further assumption is that the contribution of the interface to the total free energy of the system is proportional to the area of the interface and can be regarded as a function of the volume fractions of the phases. This approach was used to characterize the pseudoelasticity and hysteretic dissipation of a CuZnAl alloy and also for modeling the loading–unloading behavior of a CuAlNi alloy (Musolff and Sahota, 2004). A finite strain version of the model has been developed to characterize the response of a NiTi alloy (Muller and Bruhns, 2006).

Here, a combination of the approaches developed by Muller and Xu (1991) and Liang et al. (2007) is used to model the behavior of the ZnO nanowires. The transformation is decomposed into an elastic process of structural transitions between WZ and HX through a sequence of phase equilibrium states (PES) and a dissipative process of interface propagation. The elastic equilibrium transition process is modeled using strain energy functions with multiple local minima. The dissipative nature of the interface propagation process is related to the ruggedness of the energy landscape associated with elastic energy storage and release during interface motion.

3. Computational framework

The MD simulations carried out use the Buckingham potential with charge interactions (Binks and Grimes, 1993; Wolf et al., 1999). The nanowires considered are single-crystalline and wurtzite-structured, with lattice constants $a = 3.249\,\text{Å}$ and $c = 5.206\,\text{Å}$, and a growth direction along the $[0\,1\,\bar{1}\,0]$ crystalline axis (Wang, 2004a, b, c). The wire structure is generated by repeating a wurtzite unit cell along the $[2\,\bar{1}\,\bar{1}\,0]$, $[0\,0\,0\,1]$, and $[0\,1\,\bar{1}\,0]$ directions. Three different cross-sectional sizes (21.22×18.95, 31.02×29.42, and $40.81 \times 39.89\,\text{Å}$) are considered. The smallest cross-sectional size ($21.22 \times 18.95\,\text{Å}$) is chosen such that the short range cutoff distance in the Buckingham potential (Binks and Grimes, 1993; Wolf et al., 1999) is smaller than the smallest wire dimension and long-range interactions are properly considered (Kulkarni et al., 2005). Periodic boundary conditions are specified in the axial direction with a computational cell length of 150.83 Å for all the cross-sections analyzed (Kulkarni and Zhou, 2006a, b). The analyses are carried out at three temperatures (100, 300, and 500 K) to quantify the effect of temperature on the behavior.

Since the crystallographically constructed nanowires may not be in equilibrium, pre-loading relaxations are carried out for 3 ps to obtain the wires' free-standing configurations. Following the initial relaxations, a quasi-static loading scheme is employed to effect tensile deformation and to obtain the mechanical response of the nanowires. Approximate quasi-static tensile loading in each deformation increment is achieved through successive loading and equilibration. Specifically in each deformation increment, stretching at a specified rate of 0.005/ps is first carried out for 0.5 ps using a modified version of the NPT algorithm of Melchionna et al. (1993) and Spearot et al. (2005). Subsequently, with the strain maintained constant, the nanowire is relaxed for 3 ps via an algorithm for NVE ensemble (Haile, 1997) at the specified temperature. Since the loading proceeds in a series of equilibration steps, this process essentially simulates quasi-static loading of the specimen. Unloading is implemented in a similar manner with a reduction in strain for each unloading step. More details of the MD simulations can be found in Kulkarni et al. (2006, 2007) and Wang et al. (2007a).

4. Thermodynamics of loading and unloading

The process of elastic transition between equilibrium WZ and HX states is thermodynamically reversible and the process of interface propagation is thermodynamically irreversible. The reversible process involves the continuous evolution of the volume fractions of the phases with the overall strain and converts part of the mechanical work from the applied stress into bulk and interfacial strain energy. The irreversible process accounts for the dissipation associated with overcoming the energy barrier between the WZ and HX states as the transformation progresses through the propagation of the interfaces between the WZ and the HX regions.

The first law of thermodynamics relates the change in internal energy, work input and dissipation as

$$\mathrm{d}W = \mathrm{d}U + \mathrm{d}Q, \tag{1}$$

where $\mathrm{d}W$ is the work done by applied loading, $\mathrm{d}U$ is the change in internal energy in the nanowire, and $\mathrm{d}Q$ is the energy dissipated in the form of heat exchange. During the loading and unloading of single-phase nanowires (A→B, D→E, E→F, and H→A in Figs. 1(b) and (c)), there is no dissipation (i.e., $\mathrm{d}Q = 0$). Hence,

$$\mathrm{d}W = \mathrm{d}U. \tag{2}$$

However, when phase transformation occurs (B→C→D and F→G→H in Fig. 1(b) and (c)), $|\mathrm{d}Q| > 0$.

Table 1 gives the signs of the three thermodynamic quantities. In this convention, work done on the system and heat dissipated (flowing out of the system) are considered positive and vice versa. During loading, external work $\mathrm{d}W$ is positive and part of it goes toward increasing the strain energy $\mathrm{d}U$ and part of it is dissipated as heat $\mathrm{d}Q$. The relation can be written as

$$|\mathrm{d}W| = |\mathrm{d}U| + |\mathrm{d}Q|. \tag{3}$$

During unloading, the strain energy in the nanowire decreases. Part of the decrease is expended on providing work to the surroundings and part of it is dissipated as heat. The relation is

$$|\mathrm{d}W| = |\mathrm{d}U| - |\mathrm{d}Q|. \tag{4}$$

Table 1
Signs of mechanical work, internal energy, and dissipation during loading and unloading

	$\mathrm{d}W$	$\mathrm{d}U$	$\mathrm{d}Q$
Loading (WZ→HX)	+	+	+
Unloading (HX→WZ)	−	−	+

4.1. Macroscopic stress and strain

The total mechanical work is

$$W = V^0 \int_0^{\varepsilon} \sigma \, \mathrm{d}\varepsilon, \tag{5}$$

where σ and ε are the macroscopic stress and strain, respectively, and V^0 is the volume of the undeformed WZ wire. Here, the macroscopic strain ε is the nominal engineering strain relative to the undeformed WZ wire and is calculated as

$$\varepsilon = \frac{\Delta L}{L^0}, \tag{6}$$

with ΔL being the overall length change of the wire and L^0 being the length of the unstressed WZ wire. The total stress σ in the wire is

$$\sigma = \frac{1}{V^0}\frac{\partial W}{\partial \varepsilon}. \tag{7}$$

Thus, the stresses during loading and unloading are, respectively,

$$\begin{aligned} \sigma^{\mathrm{L}} &= \frac{1}{V^0}\frac{\mathrm{d}U}{\mathrm{d}\varepsilon} + \frac{1}{V^0}\frac{\mathrm{d}Q}{\mathrm{d}\varepsilon} = \sigma^{\mathrm{c}} + \sigma^{\mathrm{d}}, \quad \text{during loading and} \\ \sigma^{\mathrm{U}} &= \frac{1}{V^0}\frac{\mathrm{d}U}{\mathrm{d}\varepsilon} - \frac{1}{V^0}\frac{\mathrm{d}Q}{\mathrm{d}\varepsilon} = \sigma^{\mathrm{c}} - \sigma^{\mathrm{d}}, \quad \text{during unloading.} \end{aligned} \tag{8}$$

5. Elastic part of the behavior

5.1. Total internal energy

The framework used here is that developed by Muller (1989), Muller and Xu (1991), Raniecki and Lexcellent (1994, 1998), and Hirsinger et al. (2004). In the following discussions, subscripts 1 and 2 refer to the WZ and HX phases, respectively. The total internal energy of the system is expressed as the sum of the internal energy of WZ (U_1), the internal energy of HX (U_2), and the energy of the interface between the two phases (U_{int}). Specifically, the total energy of the system is

$$U = U_1 + U_2 + U_{\mathrm{int}}. \tag{9}$$

The internal energy of the pure phases in the phase mixture can be written as

$$U_{\mathrm{p}} = U_1 + U_2 = u_1 V_1^0 + \tilde{u}_2 V_2^0, \tag{10}$$

where u_1 is the energy density of the WZ phase reckoned over the "undeformed" volume (V_1^0) of the WZ phase at zero stress and $\tilde{u}_2$ is the energy density of the HX phase reckoned over the hypothetical free volume of the HX phase (V_2^0) at zero stress accounting for the volumetric change associated with the WZ→HX transformation. Specifically,

$$u_1 = \frac{U_1}{V_1^0} \quad \text{and} \quad \tilde{u}_2 = \frac{U_2}{V_2^0}. \tag{11}$$

At a given level of macroscopic strain ε, the total current volume of the wire is V and the current volumes of the WZ and HX regions are V_1 and V_2, respectively. For the purpose of formulating a consistent theory, it is illustrative to define the volumes V_1^0 and V_2^0 which the WZ and HX regions of the wire would assume, respectively, if they were unloaded to zero stress *with the current phase boundary held unchanged* (i.e., unloading without reverse phase transformation). For WZ, this imagined unloading is physically possible and simply involves the recovery of the elastic deformation. For HX, this imagined unloading is not possible since

the HX structure does not exist at zero stress. Here, V_2^0 is defined through

$$V_2^0 = V_1^0(1+\xi), \tag{12}$$

where ξ represents the volumetric strain associated with the WZ→HX phase transformation. This volumetric strain changes slightly with wire size and temperature and is $\xi = -4.3\%$ for a 40.81×39.89 Å wire at 100 K. For the wire size and temperature ranges analyzed, ξ is found to be between -1.6% to -4.3%. Note that the definition in Eq. (12) is rather an instrument that facilitates the formulation of relevant quantities (energy densities, in particular) relative to fixed reference states. With the above definitions, the expression in Eq. (10) can be written as

$$U_p = u_1 V_1^0 + u_2 \frac{V_2^0}{(1+\xi)}; \quad u_2 = \frac{U_2}{V_1^0}. \tag{13}$$

In the above relations, the energy densities of both phases are referred to the undeformed volume of WZ. It should be pointed out that the specific values of ξ and its size- and temperature-dependencies are implicitly accounted for in the MD calculations that yield u_1 and u_2 directly for each set of conditions.

During the transformation, conservation of mass dictates that the sum of the masses of the two phases be equal to the total mass of the nanowire, i.e.,

$$M_1 + M_2 = M, \tag{14}$$

where $M_1 = \rho_1 V_1^0$ and $M_2 = \rho_2 V_2^0$ are the masses of the WZ and HX phases, respectively, $M = \rho_1 V^0$ is the mass, and V^0 is the volume of the unstressed WZ nanowire. ρ_1 and ρ_2 are the densities of WZ and HX, respectively. Since the mass of the HX phase can also be expressed as

$$M_2 = \rho_1 \frac{V_2^0}{1+\xi}. \tag{15}$$

Eq. (14) reduces to

$$V_1^0 + \frac{V_2^0}{1+\xi} = V^0. \tag{16}$$

This states that the sum of the volumes of the untransformed WZ phase and the transformed HX phase referred to its equivalent volume in the WZ state are equal to the original undeformed volume of the wire. Eq. (16) can also be written as

$$\frac{V_1^0}{V^0} + \frac{V_2^0}{V^0(1+\xi)} = 1, \tag{17}$$

where the terms on the left-hand side represent the volume fractions of the WZ and HX phases, respectively. Eqs. (13) and (17) combine to give the total strain energy density of the pure phases (u_p) as

$$u_p = (1-f)u_1 + f u_2, \tag{18}$$

where $f = V_2^0/[V^0(1+\xi)]$ is the volume fraction of the HX phase.

5.2. Internal energy of WZ and HX phases

The internal energy densities of the WZ- and HX-structured nanowires (u_1 and u_2) as functions of their respective strains are critical in the modeling of the phase transformation, since they determine the relative stability of the two phases and the evolution of the transformation. In nanowires, the internal energy depends not only on the bulk structure and deformation but also on surface orientations and surface energies. Due to the high surface-to-volume ratios, surface energy constitutes a major portion of the total configurational energy. The surface energy and the internal energy of a nanowire are functions of wire size. This phenomenon is different from what is the case for bulk materials whose internal energy depends solely on strain. In addition, it is useful to note that the internal energy does not vanish at zero strain (or zero stress). Here, the strain is defined relative to the equilibrium bulk state. As shown by Sander (2003), the surface energy curve has

a positive slope at zero surface strain, indicating that the minimum surface energy occurs at a compressive surface strain. This is a consequence of the reduced charge transfer and imbalance of ionic forces on surfaces where atoms have fewer neighbors relative to those in the core. As a result, WZ-structured nanowires undergo relaxation through surface reconstruction and adjustment of interior lattice spacing, leading to lower overall configurational energy. In this paper, this relaxed state is taken as the reference state. The strain in the WZ structure (ε_1) defined with respect to this reference state is

$$\varepsilon_1 = \frac{l_1 - l_1^0}{l_1^0}, \tag{19}$$

where l_1 and l_1^0 are the current and reference lengths. For the HX phase, special considerations similar to those in the definition of V_2^0 are required. Since HX does not exist at zero stress, the strains in the HX phase are defined relative to the reference length of

$$l_2^0 = l_1^0(1+\eta). \tag{20}$$

Here, η is the longitudinal strain associated with the WZ-to-HX transformation and, according to MD calculations, has values in the range of 2.3–4.3% for the wire sizes and temperatures analyzed. With the reference state, the strain in HX is defined as

$$\varepsilon_2 = \frac{l_2 - l_2^0}{l_2^0}. \tag{21}$$

The internal energy density of each phase is expressed as

$$u_i = u_i^0 + u_i^{\varepsilon}(\varepsilon_i), \quad i = 1, 2. \tag{22}$$

Here, u_i^0 is the energy of formation, $u_i^{\varepsilon}(\varepsilon_i)$ is the strain energy density, and ε_i is the strain of the ith phase. The formation energy depends on temperature and the elastic constants are functions of both temperature and strain.

The one-dimensional nature of the wires and the uniaxial tensile loading permit the use of 1D internal energy functions. For each phase, the strain energy density at each wire size and each temperature is obtained through MD calculations. The strain energy functions thus developed account for the effects of temperature and size (through explicit inclusion of surfaces in the MD model), allowing the size- and temperature-dependence of wire responses to be analyzed. Fig. 2 shows the internal energy densities of WZ and HX structures for a 40.81 × 39.89 wire at 100 K. The formation energies of the two phases are indicated. Note that the formation energy of WZ is lower than that of HX, consistent with the fact that WZ is the natural state of the wires at 100 K without external loading.

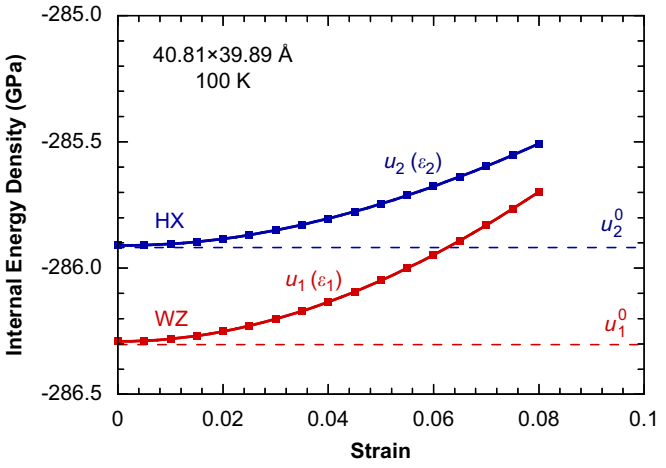

Fig. 2. Internal energy density functions of a 40.81 × 39.89 Å wire in WZ and HX states at 100 K.

5.3. Interfacial energy

Interfacial energy includes contributions from the formation energy of the interface, elastic misfit of the phases and elastic interactions of neighboring domains. Its accurate evaluation is somewhat complicated and various methods have been proposed in the literature (Gall et al., 2000; Muller and Bruhns, 2006), primarily due to complex geometry and anisotropy. Here, the phenomenological approach developed by Muller and Xu (1991) is adopted. Specifically, the interfacial energy density is written as

$$u_{\text{int}} = \frac{U_{\text{int}}}{V^0} = 4f(1-f)u_{\text{int}}^{\text{m}}, \tag{23}$$

where $u_{\text{int}}^{\text{m}}$ is the maximum value when the wire is evenly divided by the WZ and HX phases ($f = 0.5$). Obviously, $4f(1-f) = u_{\text{int}}/u_{\text{int}}^{\text{m}} = S_{\text{int}}/S_{\text{int}}^{\text{m}}$ denotes both the normalized interfacial energy $u_{\text{int}}/u_{\text{int}}^{\text{m}}$ and the normalized interfacial area $S_{\text{int}}/S_{\text{int}}^{\text{m}}$ (Muller and Xu, 1991). Here, S_{int} is the interfacial area at a prescribed value of macroscopic strain ε and $S_{\text{int}}^{\text{m}}$ is its corresponding maximum value at $f = 0.5$. Note that u_{int} vanishes at $f = 0$ and 1. One underlying assumption of Eq. (23) is that the orientation dependence of interfacial energy is negligible and the interfacial energy is only a function of the interfacial area. Fig. 3 provides a comparison of the model prediction and the MD result of $u_{\text{int}}/u_{\text{int}}^{\text{m}}$ as a function of strain for a 40.81×39.89 Å wire at 100 K. A very good agreement is seen between the model prediction and the MD data. The part of the profile from the model between $\varepsilon = 0.04$ and 0.072 is not physical and not observed in MD since the model does not account for the energy barrier for the WZ-to-HX transformation. More discussion on this will be given in Section 6.

5.4. Constrained energy minimization

The total internal energy density resulting from Eq. (9) is

$$u = (1-f)u_1 + fu_2 + 4f(1-f)u_{\text{int}}^{\text{m}}. \tag{24}$$

The macroscopic strain ε includes contributions from the elastic strains in the phases (ε_1 and ε_2) and the transformation strain (η) and can be obtained by invoking the rule of mixture as

$$\varepsilon = (1-f)\varepsilon_1 + f\varepsilon_2 + f\eta. \tag{25}$$

Obviously, in Eq. (24), the independent state variables are ε_1, ε, and f. At any given level of macroscopic strain ε, minimization of the total energy density in Eq. (24) under the constraint of Eq. (25) yields the equilibrium condition that defines the equilibrium state (specified by ε_1, ε_2, and f) of the transforming

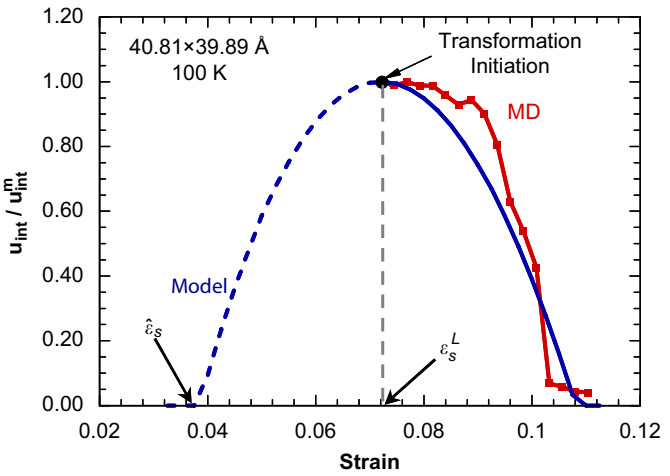

Fig. 3. Comparison of model prediction and MD result for the normalized interfacial energy as a function of macroscopic strain for a 40.81×39.89 Å wire at 100 K.

nanowire. When carried over the entire range of ε, this constrained minimization process yields the full equilibrium path for both the forward WZ-to-HX and the reverse HX-to-WZ transformations. The equilibrium transformation path so obtained for the 40.81×39.89 Å wire at 100 K as measured by f as a function of ε is shown in Fig. 4. Initially for $\varepsilon < 0.04$, $f = 0$ and the wire exists solely in the WZ phase. At $\varepsilon = \hat{\varepsilon}_s = 0.04$, the WZ-to-HX transformation initiates. Note, however, that $\hat{\varepsilon}_s$ is not equal to the actual transformation initiation strain observed in MD simulations (ε_s^L in Fig. 1(c)). This difference arises from the fact that the equilibrium analysis does not account for the energy barrier for the forward WZ-to-HX transformation. The actual transformation initiation occurs at ε_s^L in (Figs. 1(c) and 3). As the transformation progresses, the volume fractions of the two phases evolve smoothly. The transformation is complete at $\varepsilon = \varepsilon_c = 0.11$ for the wire in Figs. 3–5. Further deformation beyond ε_c corresponds to the purely elastic stretch of the HX-structured wire with $f = 1$.

5.5. Stress associated with the equilibrium transformation process (σ_c)

During the transformation, the equilibrium part of the stresses in the phases is

$$\sigma_1 = \frac{\partial u_1}{\partial \varepsilon_1} \quad \text{and} \quad \sigma_2 = \frac{\partial u_2}{\partial \varepsilon_2}. \tag{26}$$

The stress associated with the equilibrium transformation process is then (Eq. (8))

$$\begin{aligned}
\sigma_c &= \frac{1}{V_0}\left(\frac{\partial U}{\partial \varepsilon}\right) \\
&= \frac{1}{V_0}\left(\frac{\partial U_p}{\partial \varepsilon}\right) + \frac{1}{V_0}\left(\frac{\partial U_{int}}{\partial \varepsilon}\right) \\
&= \frac{1}{V_0}\frac{\partial}{\partial \varepsilon}(u_1 V_1^0) + \frac{1}{V_0}\frac{\partial}{\partial \varepsilon}\left[u_2 \frac{V_2^0}{(1+\xi)}\right] + \frac{1}{V_0}\frac{\partial}{\partial \varepsilon}[4f(1-f)u_{int}^m] \\
&= \frac{\partial}{\partial \varepsilon}[u_1(1-f)] + \frac{\partial}{\partial \varepsilon}(u_2 f) + 4(1-2f)u_{int}^m \frac{\partial f}{\partial \varepsilon} \\
&= (1-f)\frac{\partial u_1}{\partial \varepsilon_1}\frac{\partial \varepsilon_1}{\partial \varepsilon} + f\frac{\partial u_2}{\partial \varepsilon_2}\frac{\partial \varepsilon_2}{\partial \varepsilon} + \frac{\partial f}{\partial \varepsilon}(u_2 - u_1) + 4(1-2f)u_{int}^m \frac{\partial f}{\partial \varepsilon} \\
&= (1-f)\left(\frac{\partial \varepsilon_1}{\partial \varepsilon}\right)\sigma_1 + f\left(\frac{\partial \varepsilon_2}{\partial \varepsilon}\right)\sigma_2 + \frac{\partial f}{\partial \varepsilon}(u_2 - u_1) + 4(1-2f)u_{int}^m \left(\frac{\partial f}{\partial \varepsilon}\right).
\end{aligned} \tag{27}$$

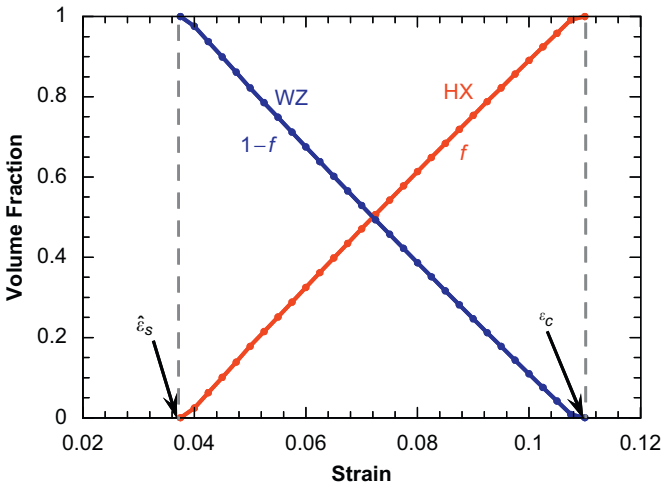

Fig. 4. Evolution of the volume fractions of WZ and HX during tensile loading as predicted by the model for a 40.81×39.89 Å wire at 100 K.

Here, ε_1, ε_2, $\partial\varepsilon_1/\partial\varepsilon$, $\partial\varepsilon_2/\partial\varepsilon$, and f as functions of ε are determined from the constrained energy minimization process discussed in Section 5.4.

σ_c describes the thermodynamically reversible part of the deformation process. Note that Eq. (27) is also applicable to the wire as it deforms fully elastically in the WZ state before the initiation of the transformation ($f=0$) and in the HX state after the completion of the transformation ($f=1$). For example, for the loading and unloading of a single phase WZ wire, $f=0$, $\partial f/\partial\varepsilon=0$, and $\partial\varepsilon_1/\partial\varepsilon=1$. Consequently, the stress reduces to that in the WZ phase, i.e., $\sigma=\sigma_1$. Similarly, for the elastic loading and unloading of a single phase HX wire, $f=1$, $\partial f/\partial\varepsilon=0$, $\partial\varepsilon_2/\partial\varepsilon=1$, and $\sigma=\sigma_2$.

Note that σ_c only captures the equilibrium part of the transformation process, since the nanowire goes through a sequence of unstable and equilibrium states (more discussions in Section 6). For example, the stress–strain response of the 40.81×39.89 Å wire at 100 K is given in Fig. 5. Both the MD data and the model prediction for σ_c are shown. The MD profile shows alternate stages of stress increases (toward unstable states) and decreases (toward equilibrium states) during loading and alternate stages of stress decreases (toward unstable states) and increases (toward equilibrium states) during unloading. Obviously, σ_c is close to the valleys in loading and the peaks in unloading since these valleys (loading) and peaks (unloading) correspond to more relaxed states of the nanowire.

6. Dissipative process of interface propagation

The thermodynamically irreversible part of the phase transformation event involves contributions from barriers for both the initiation and propagation of the transformation through the nucleation and motion of interfaces. A schematic illustration of the energy and stress profiles associated with the process is given in Fig. 6. The initiation of transformation occurs at the formation of the first nucleus of the HX phase (forward WZ-to-HX transformation during loading) or the WZ phase (reverse HX-to-WZ transformation during unloading). The stress at which the WZ-to-HX transformation initiates (point B, Fig. 1(c)) can be obtained from the value of ε_s^L and the constitutive behavior of the WZ phase (Fig. 2). Similarly, the stress at which the HX-to-WZ transformation initiates (point F, Fig. 1(c)) can be obtained from the value of ε_s^U and the constitutive behavior of the HX phase (Fig. 2). Since the elastic behaviors for $\varepsilon<\varepsilon_s^L$ (A↔B, Fig. 1(c)) and $\varepsilon>\varepsilon_s^U$ (F↔E, Fig. 1(c)) are also fully described by the single phase responses of the WZ and HX wires, respectively, the discussion on the dissipative process of interfacial propagation concerns only the deformation stages of B→C→D (loading) and F→G→H (unloading).

The propagation of phase boundaries after phase nucleation involves a sequence of unstable and stable states. This process is a consequence of the ruggedness of the energy profiles associated interface propagation. For example, during loading, the nanowire initially stores energy (C→P in Fig. 6(a)) and is brought to

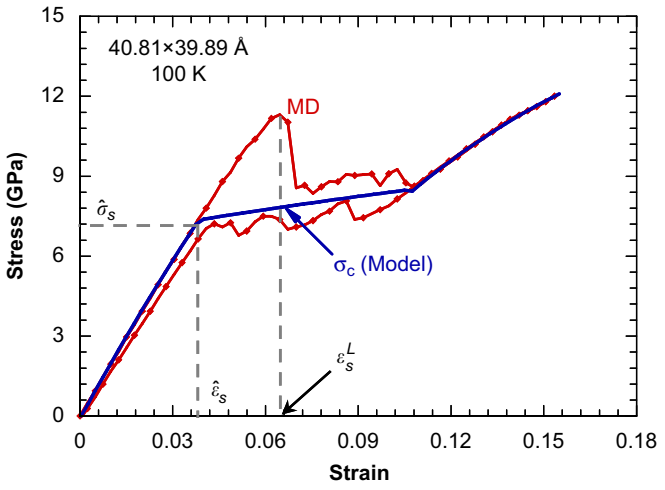

Fig. 5. Comparison of σ_c and the full stress–strain hysteresis for a 40.81×39.89 Å wire at 100 K.

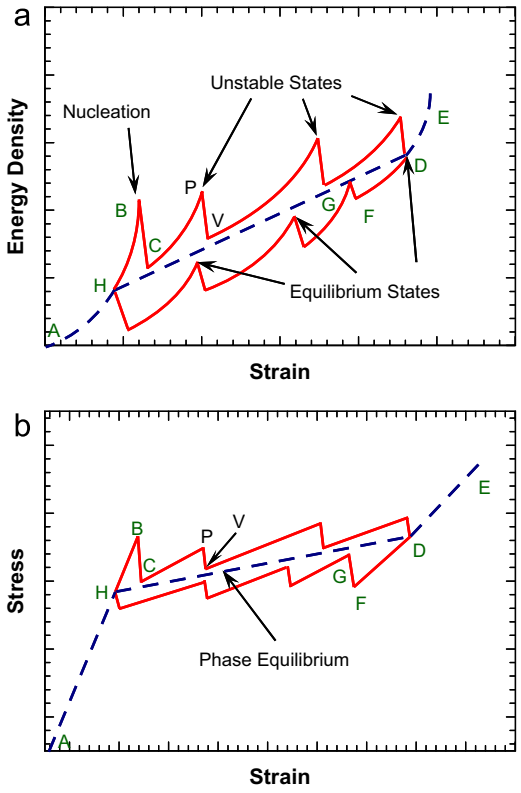

Fig. 6. A schematic illustration of the variations of (a) the internal energy density and (b) the stress.

an unstable high-energy state (point P in Fig. 6(a)). At point P, the wire reaches instability and further nucleation of the HX phase takes place, resulting in the propagation of the phase boundary. This structural change is accompanied by a drop in energy U from its value at point P to the value at point V, bringing the wire closer to the more relaxed equilibrium state represented by the dotted line. The released energy ($\Delta U = U^{\mathrm{P}} - U^{\mathrm{V}}$) is dissipated as heat and constitutes part of the dissipation $\Delta Q^{\mathrm{P}\to\mathrm{V}}$ as defined in Eq. (1).

During this period of "energy accumulation and release", stress σ first increases between C and P and decreases precipitously between P and V (Fig. 6(b)). The stress at V may approach σ_{c} in Eq. (27). Fig. 7 shows several configurations in the stage of $0.075<\varepsilon<0.084$ of the nanowire referred to in Figs. 3 and 5. These pictures show states of the wire immediately after the initiation of the WZ-to-HX transformation. Obviously over this stage (strain up to 0.08, first three frames with $f = 0.453$, 0.458, and 0.461), the structure of the wire remains essentially unchanged without significant progression of transformation in either direction (therefore, without significant dissipation), while at the same time the mechanical work input is converted into strain energy and stored in the wire. As soon as the strain exceeds 0.08, the interface starts to propagate and clear progression of the WZ-to-HX transformation occurs (note the difference between $f = 0.461$ and 0.54). This process is a direct reflection of the ruggedness of the energy landscape discussed earlier.

Just as the interfacial energy can be regarded as being proportional to the interfacial area, the energy required to move the WZ-to-HX phase boundaries naturally increases with the size of the interface, leading to a dependence of the dissipative stress (σ_{d}) on the size of the phase boundary which changes as the transformation progresses. To reflect this dependence, σ_{d} is assumed to be proportional to the normalized interfacial area fraction $S_{\mathrm{int}}/S_{\mathrm{int}}^{\mathrm{m}}$ and varies with f according to

$$\sigma_{\mathrm{d}} = 4f(1-f)\sigma_{\mathrm{d}}^{\mathrm{m}}. \tag{28}$$

Here, $\sigma_{\mathrm{d}}^{\mathrm{m}}$ is the maximum value of σ_{d} which occurs at $f = 0.5$. The history of σ_{d} is shown in Fig. 8(a) and the history of energy dissipated per unit volume $q = Q/V^0$ is shown in Fig. 8(b). For comparison, the history of f

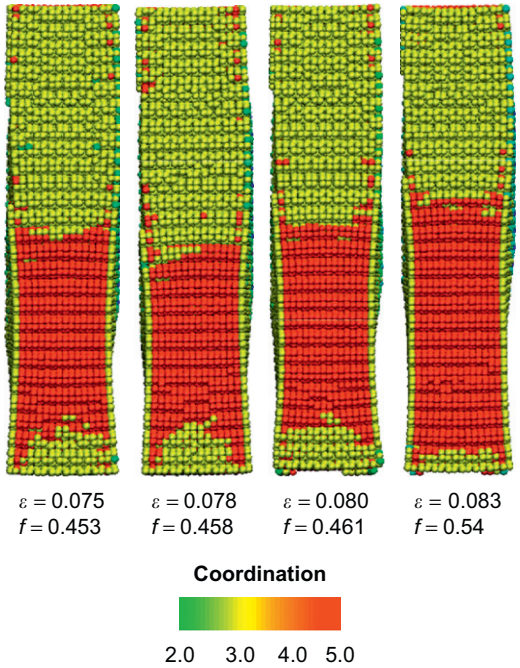

Fig. 7. Configurations of a 40.81×39.89 Å wire during loading at 100 K. The volume fraction f is essentially constant for $\varepsilon \leqslant 0.08$ and increases rapidly once ε exceeds 0.08.

as a function of ε for the nanowire referred to in Figs. 3 and 5 is also shown. Note that $\sigma_d = 0$ for $f = 0$ ($\varepsilon \leqslant \hat{\varepsilon}_s$) and $f = 1$ ($\varepsilon \geqslant \hat{\varepsilon}_c$).

7. Macroscopic stress σ

Eqs. (8), (27), and (28) combine to give the macroscopic stress as

$$\begin{aligned}\sigma &= \frac{1}{V_0}\left(\frac{\partial U}{\partial \varepsilon}\right) \pm \frac{1}{V_0}\left(\frac{\partial Q}{\partial \varepsilon}\right) \\ &= \underbrace{(1-f)\left(\frac{\partial \varepsilon_1}{\partial \varepsilon}\right)\sigma_1 + f\left(\frac{\partial \varepsilon_2}{\partial \varepsilon}\right)\sigma_2 + \frac{\partial f}{\partial \varepsilon}(u_2 - u_1) + 4(1-2f)u_{\text{int}}^{\text{m}}\left(\frac{\partial f}{\partial \varepsilon}\right)}_{\sigma^{\text{c}}} \pm \underbrace{4f(1-f)\sigma_{\text{d}}^{\text{m}}}_{\sigma^{\text{d}}},\end{aligned} \tag{29}$$

where the positive and negative signs correspond to loading and unloading, respectively.

Note that the total stress reduces to the stresses in the corresponding individual phases during the elastic deformation in the WZ state ($\sigma = \sigma_1$) before the initiation of the WZ→HX transformation ($f = 0$) and in the HX state ($\sigma = \sigma_2$) after the completion of the HX→WZ transformation ($f = 1$). During the transformations ($0 < f < 1$), the total stress represents the overall response of the transforming wire, accounting for contributions from the elasticity of the two constituent phases, the structural energy of the evolving interface between the two phases, and the dissipation associated with the nucleation, propagation and annihilation of the interface.

As previously discussed, MD simulations show that the WZ→HX and HX→WZ transformations occur in a "stick-and-slip" manner, involving alternating stages of primarily elastic deformations in the phases without appreciable interface propagation and stages of rapid interface propagation (progression of phase transformation, Fig. 7). This intermittent process of elastic deformation (accumulation of strain energy) and transformation progression (release of strain energy) leads to serrated stress–strain relations, as shown

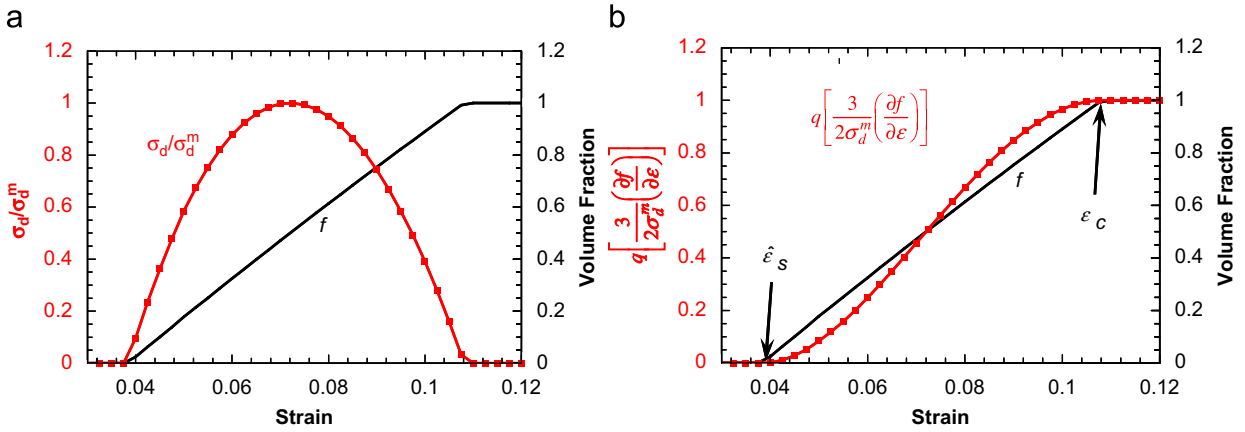

Fig. 8. Evolution with strain during transformation of (a) normalized stress associated with dissipation and (b) normalized energy dissipated.

and illustrated in Figs. 5 and 6. It is a fundamental reflection of the discrete nature of the crystalline lattice, the existence of energy barriers between the WZ and HX crystalline structures (energy landscape with multiple local minima), and the small sizes of the nanowires. In particular, the fact that the energy landscape involves multiple local minima plays a dominant role, as shown by, e.g., Fedelich and Zanzotto (1992) and Truskinovsky and Vainchtein (2004). Similar serrated stress–strain relations have been observed and analyzed in other low-dimensional nanomaterials such as metal nanowires (Liang et al., 2007), although the serrations can be averaged out and, therefore, not observed at the macroscopic level. Prediction of the rugged stress–strain profiles at the continuum level requires a detailed characterization of the energy landscapes not only for the equilibrium transition between the WZ and HX structures but also for the interfacial nucleation and annihilation. The model developed here focuses on the delineation of the thermodynamically reversible and irreversible processes of the transformations. The interest is primarily in the elucidation of the mechanisms behind the novel pseudoelastic behavior at the nanoscale, rather than in a full account of the serrations in the stress–strain relations. It is important to point out that it is possible to obtain a phenomenological characterization of the rugged stress–strain profiles within the framework of the model developed here. One such attempt would involve, for example, accepting as input from MD simulations values of the phase volume fraction f at which the phase transformations stop and restart. Such an analysis is currently being carried for FCC metal nanowires and for ZnO nanowires. The results may be reported in a future publication.

8. Comparison with MD results

The stress–strain relation predicted by the model and that obtained from MD simulations for the 40.81×39.89 Å wire at 100 K are shown in Fig. 9. As part of the input to the model, the constitutive behaviors of the two phases are determined by MD calculations, as detailed in Section 5.2. The elastic part of the stresses (σ_i) and the strain (ε_i) in each phase, the derivatives of the strains ($\partial\varepsilon_i/\partial\varepsilon$) and the volume fraction f at each ε are calculated through constrained energy minimization. The model developed here has two independent parameters ($u_{\text{int}}^{\text{m}}$ and $\sigma_{\text{d}}^{\text{m}}$). The maximum interfacial energy density ($u_{\text{int}}^{\text{m}}$) is related to the evolution of equilibrium states and is determined through fitting to MD results for each size and temperature. The value of $u_{\text{int}}^{\text{m}}$ which varies with temperature and size determines the phase equilibrium stress during the evolution of the transformation for various wire sizes and temperatures. On the other hand, the maximum value of the dissipative stress ($\sigma_{\text{d}}^{\text{m}}$) is related to the dissipation associated with interface propagation and its value determines the size of the hysteresis loop in a loading–unloading cycle. The value of $\sigma_{\text{d}}^{\text{m}}$ is also determined by fitting to MD results for the wire sizes and temperatures considered. The individual contributions to the macroscopic stress associated with the WZ-to-HX forward transformation are compared

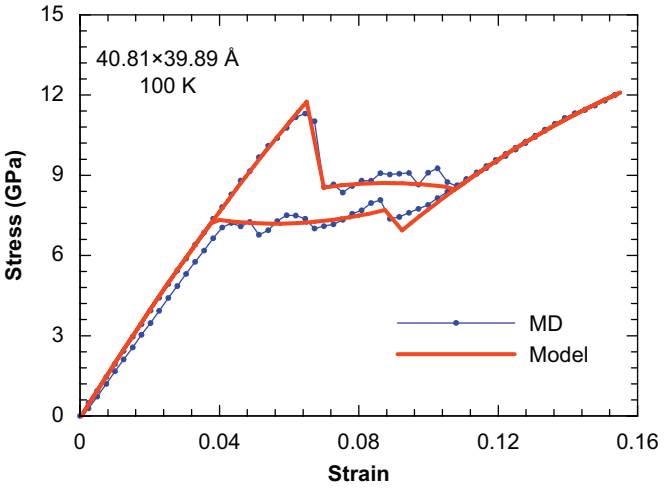

Fig. 9. Comparison of the stress–strain relations of a 40.81×39.89 Å wire at 100 K as predicted by the model and obtained from MD calculation.

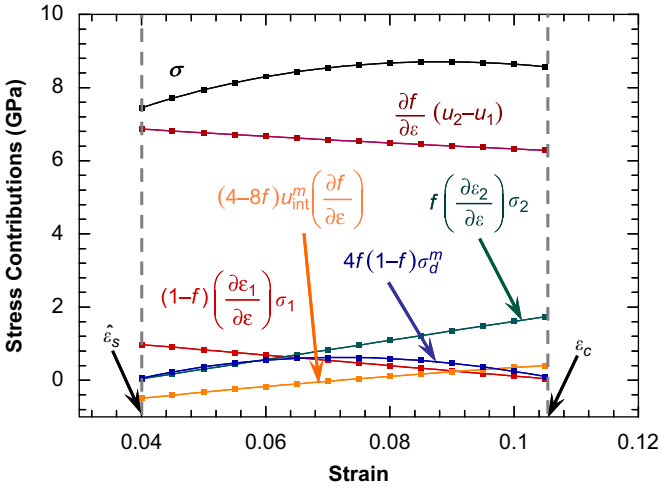

Fig. 10. Contributions to the total stress by terms in Eq. (29).

in Fig. 10. The primary contribution (~83%) comes from the gradient term $\partial f/\partial \varepsilon(u_2 - u_1)$ which decreases slightly as ε increases, reflecting the fact that most of the external work dW is converted into the internal energy of the HX phase. The contributions of the other terms are relatively small. The term $(1-f)(\partial \varepsilon_1/\partial \varepsilon)\sigma_1$ decreases as the volume fraction of the HX phase increases, while the term $f(\partial \varepsilon_2/\partial \varepsilon)\sigma_2$ shows a gradual increase. The dissipative stress σ_d first increases and then decreases. The contribution from the interfacial energy $4(1-2f)u_{\text{int}}^m(\partial f/\partial \varepsilon)$ is also quite small (<7% of the overall stress) throughout the transformation.

The relative magnitudes of these terms affect the size and temperature dependence of the behavior of the wires. To quantify the effects, the micromechanics framework developed here is used to analyze the pseudoelastic behavior of wires with the lateral dimensions of 21.22×18.95, 31.02×29.42, and 40.81×39.89 Å over the temperature range of 100–500 K. The internal energy functions of the WZ and HX phases for these sizes and temperatures are calculated using MD simulations. The model predictions and MD results are shown in Fig. 11. Excellent agreement is seen for all the cases analyzed. Obviously, the

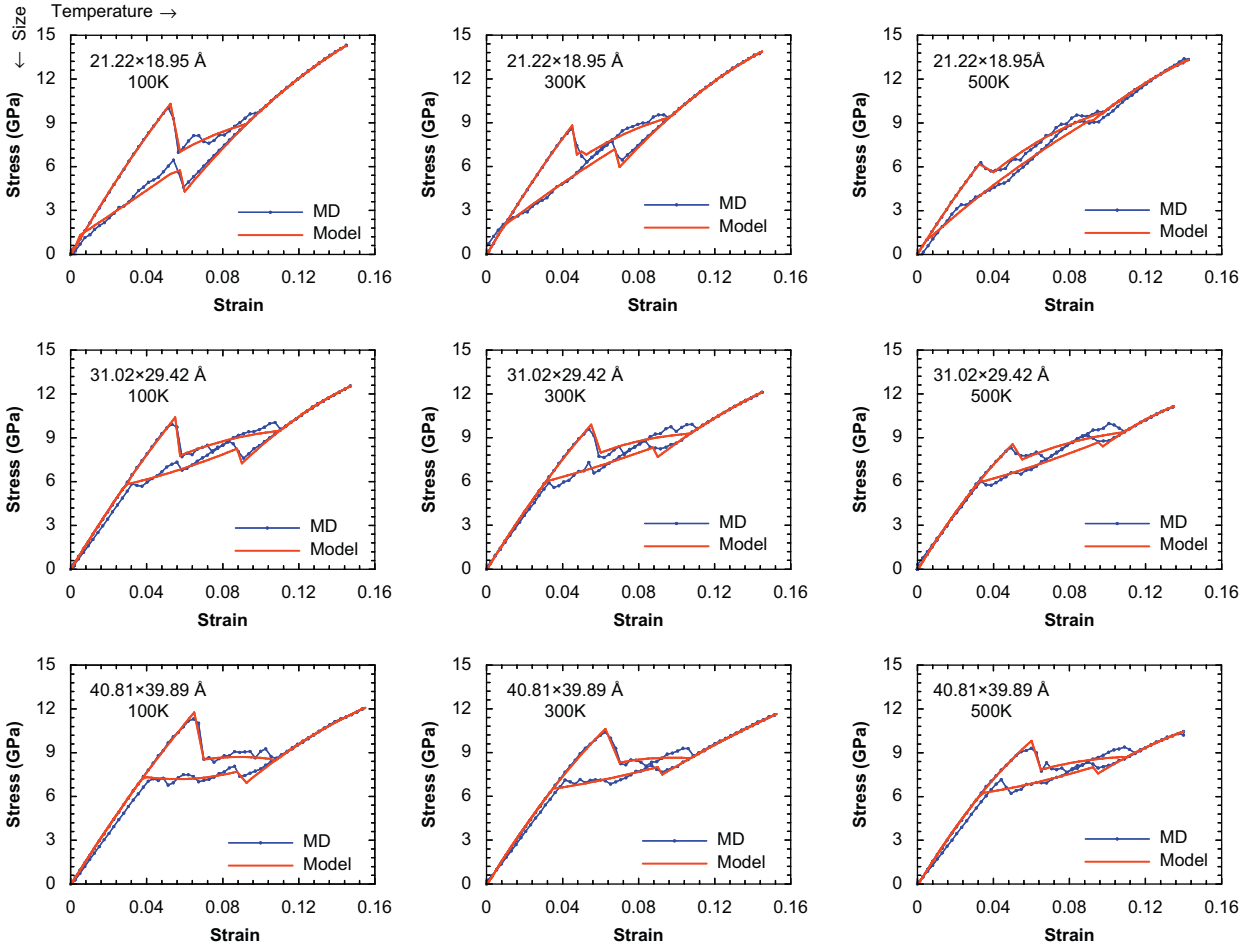

Fig. 11. Comparison of the stress–strain relations of three wire sizes at three temperatures as predicted by the model and obtained from MD calculations.

model captures the overall characteristics of the behaviors of the wires and correctly accounts for the size and temperature effects.

8.1. Size and temperature effects

To analyze the effects of size and temperature, the responses of three wire sizes (21.22×18.95, 31.02×29.42, and 40.81×39.89 Å) at 300 K and the response of a 31.02×29.42 Å wire at three temperatures are considered.

The effect of wire size on response is analyzed in Fig. 12(a) (loading) and (b) (unloading). The MD results shown are obtained for a temperature of 300 K. The elastic moduli in the elastic stages of deformation increase with wire size, owing to the higher surface-to-volume ratios at smaller sizes. This stiffening effect can be explained by the strain energy profiles for WZ (Fig. 12(c)) and HX (Fig. 12(d)). The size-dependence is more pronounced for the HX structure, primarily because the energy densities of the surfaces of HX wires are higher than the energy densities of the surfaces of the WZ wires. The critical stresses for transformation initiation decrease as wires size decreases. Again, the effect of surfaces is at work and the mechanism has to do with the fact that the structure of reorganized (0 0 0 1) side surfaces of WZ wires have atomic configurations similar to those of the surfaces of HX-structured wires, as previously observed by Claeyssens et al. (2005) and Freeman et al. (2006) in both experiments and first principles calculations. The similarity in surface behaviors between

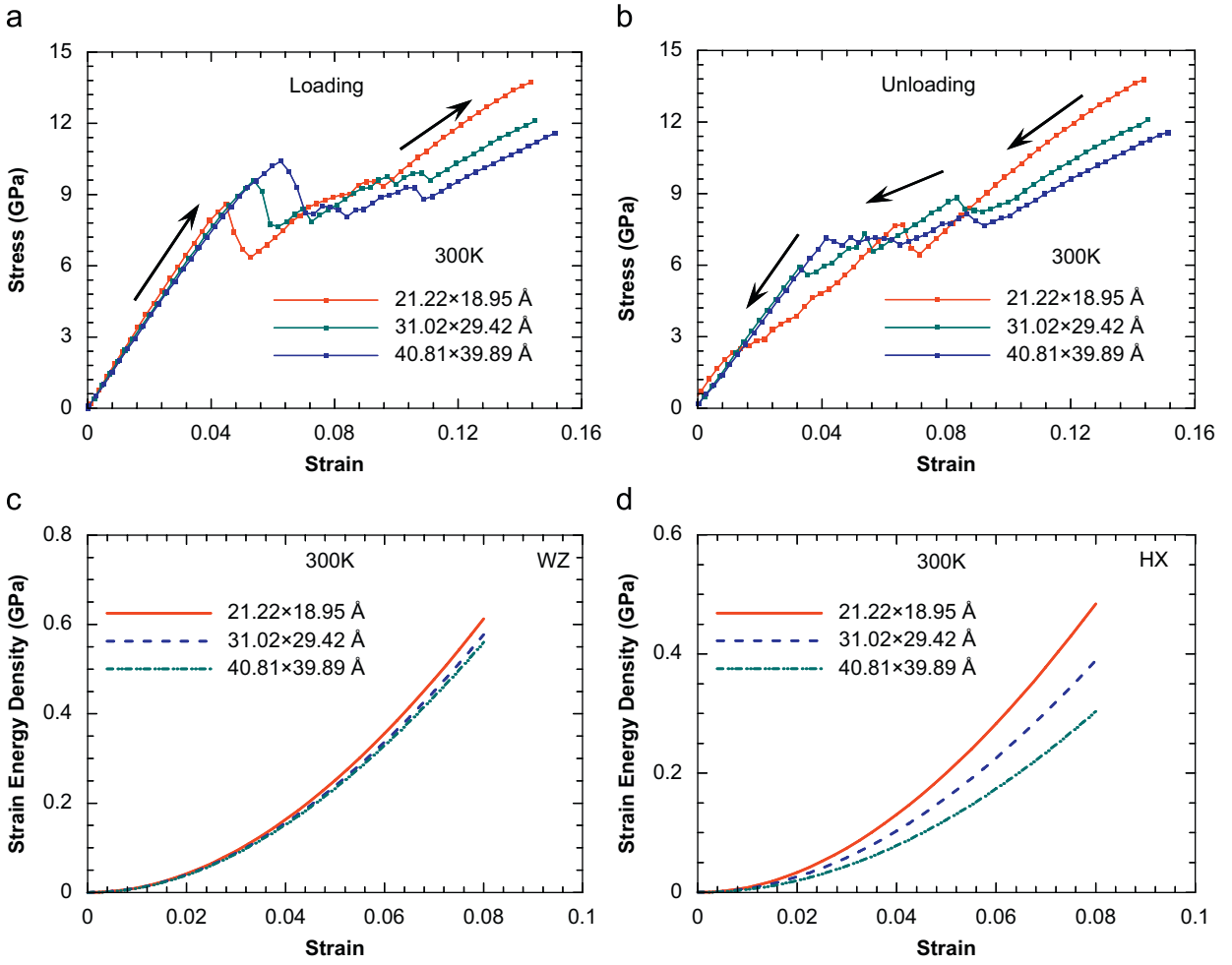

Fig. 12. Stress–strain relations for wires of three different lateral sizes at 300 K, (a) loading, (b) unloading, (c) strain energy function for the WZ phase, and (d) strain energy function for the HX phase.

WZ- and HX-structured wires allows bulk behavior to dominate the transformation process. The higher surface-to-volume rations at smaller wire sizes reduce the effect of the wire core, causing the critical stresses to decrease with size, despite the fact the formation energy difference between HX and WZ wires (Δu^0) is slightly higher at smaller wires sizes (Fig. 13(a)). This effect can be phenomenologically seen from the values of the maximum interfacial energy $u_{\text{int}}^{\text{m}}$ in Fig. 13(b) and the values of $\hat{\sigma}_{\text{s}}$ (the stress corresponding to the strain of $\varepsilon = \hat{\varepsilon}_{\text{s}}$ (Fig. 5) at which the two phases are equally favored under equilibrium conditions) in Fig. 13(c). Finally, it is worthwhile to note that the dissipative process of interfacial propagation does not have an appreciable contribution to the size dependence of the overall wire response, as can be seen from Fig. 13(d) which relates $\sigma_{\text{d}}^{\text{m}}$ to wire size.

The responses of a 31.02×29.42 Å wire at 100, 300, and 500 K are shown in Fig. 14(a) (loading) and (b) (unloading). There is a moderate decrease in stress at higher temperatures. This thermal softening arises from both changes in the constitutive response of the WZ and HX phases and changes in the difference between the energy barriers for the transformations and available thermal energy in the system. The first aspect can be quantified explicitly. Fig. 14(c) and (d) show, respectively, the strain energy profiles for WZ and HX at 100, 300, and 500 K. The dependence on temperature is a weak one and is more appreciable at large strains. The dependence of the formation energy densities (u_i^0) of WZ and HX on temperature over the range of 100–500 K is shown in Fig. 15(a). While the actual values of u_i^0 affect phase stability, the difference $\Delta u^0 = u_2^0 - u_1^0$

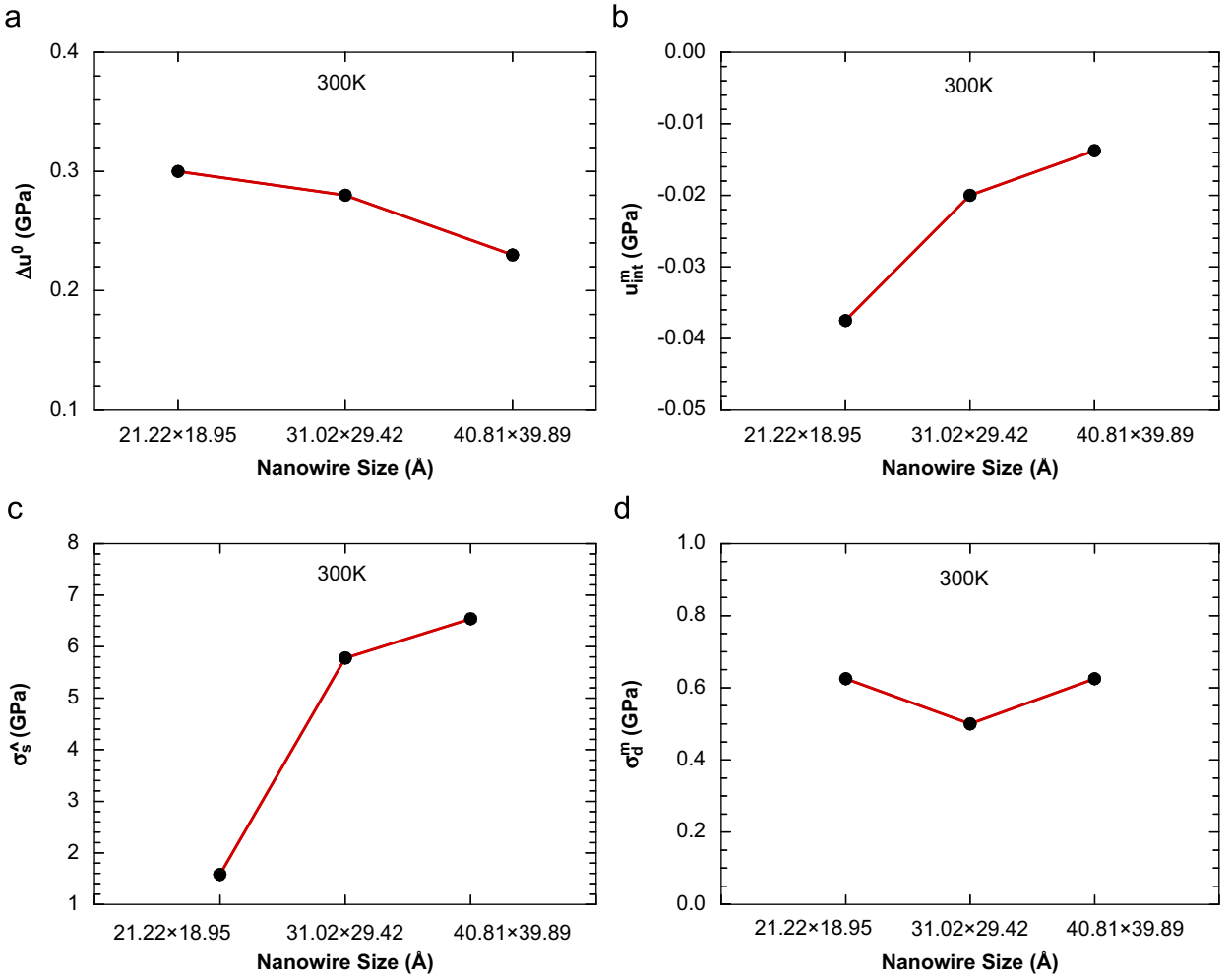

Fig. 13. Variation with wire size of (a) formation energy difference (Δu^0) between the WZ and HX structures, (b) maximum interfacial energy ($u_{\text{int}}^{\text{m}}$), (c) equilibrium transition stress ($\hat{\sigma}_s$), and (d) maximum stress associated with energy dissipation ($\sigma_{\text{d}}^{\text{m}}$).

influences the total stress during transformation. This can be clearly seen in the term $(u_2 - u_1)\partial f/\partial\varepsilon$ (Fig. 10) which depends on Δu^0. For the 31.02×29.42 Å wire, Δu^0 is only weakly temperature-dependent, suggesting that it is not the primary source of the temperature dependence of the transformation stress.

The dependence of the transformation stress on temperature arises primarily out of the dissipative part of the transformation process, as can be seen from the maximum stress associated with dissipation ($\sigma_{\text{d}}^{\text{m}}$) which shows a clear dependence on temperature (Fig. 15(b)). Obviously, $\sigma_{\text{d}}^{\text{m}}$ decreases as higher thermal energy levels at higher temperatures reduce the mechanical work required to overcome the barriers for interface propagation both during loading and unloading.

Finally, it is worth noting that the maximum interfacial energy ($u_{\text{int}}^{\text{m}}$) is rather constant over the temperature range analyzed, suggesting that the interface does not contribute significantly to the temperature dependence of the pseudoelastic behavior of the wires and the temperature effect primarily comes from the bulk processes already discussed.

9. Summary

A continuum model is developed to characterize the novel pseudoelastic behavior recently discovered in ZnO nanowires. The model describes and quantifies the full cycle of behavior observed in MD simulations,

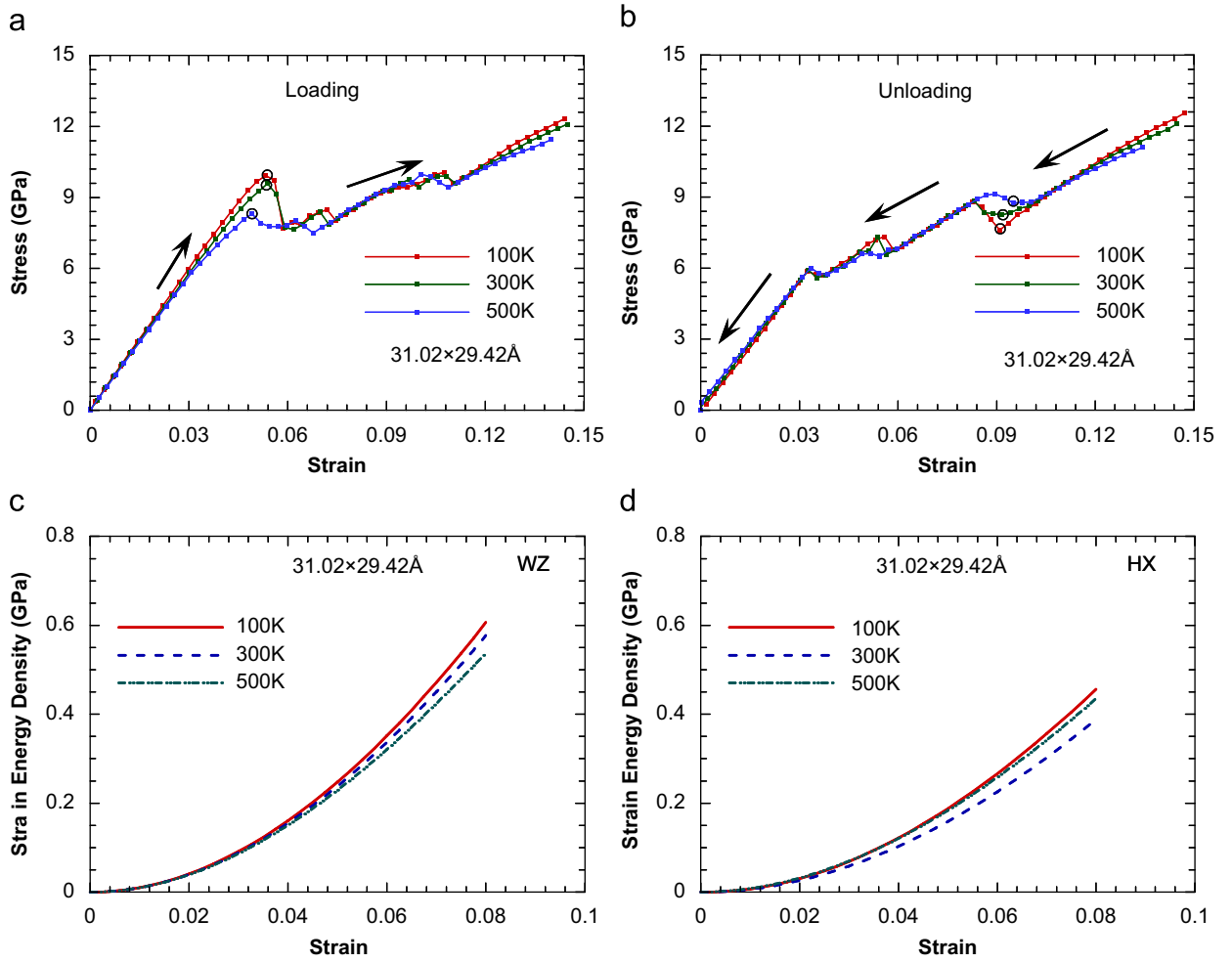

Fig. 14. Dependence of response on temperature of a 31.02×29.42 Å wire, (a) stress–strain relations during loading, (b) stress–strain relations during unloading, (c) strain energy density function for the WZ phase, and (d) strain energy density functions for the HX phase.

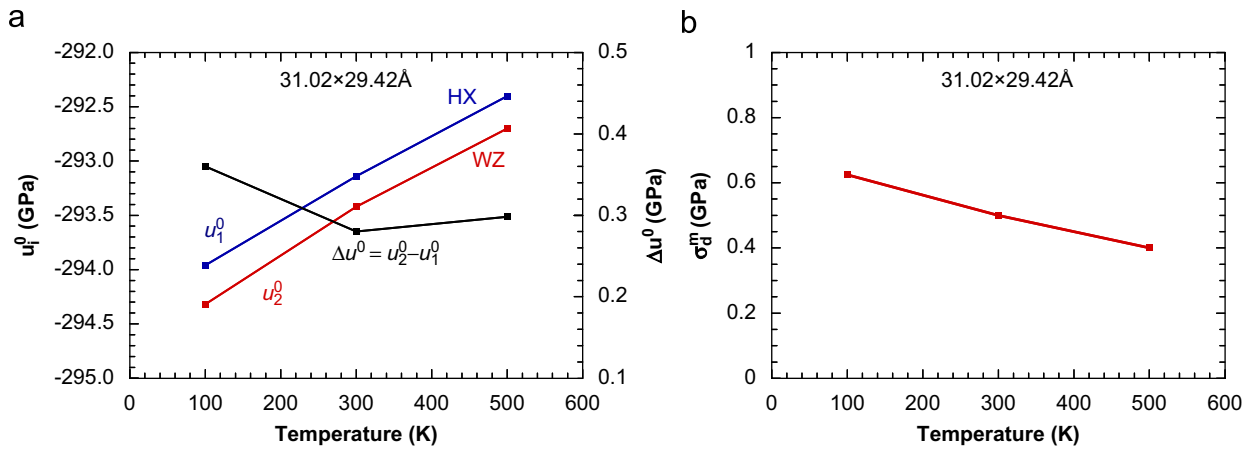

Fig. 15. Dependence on temperature of (a) the formation energy densities (u_i^0) of WZ and HX phases and the difference between them (Δu^0) and (b) the maximum stress associated with dissipation (σ_d^m).

including the elastic responses of the WZ and HX wires and the transformations between the WZ and HX phases which underlie the pseudoelastic response. The processes of phase initiation and interface propagation for both the forward WZ-to-HX transformation and reverse HX-to-WZ transformation are characterized phenomenologically using phase volume fractions. Based on the first law of thermodynamics, the model decomposes the transformation event into a thermodynamically reversible process of the evolution of phase equilibrium states and a thermodynamically irreversible process of interface nucleation and propagation. The first part is conservative and the second part accounts for the dissipation associated with the deformation in both loading and unloading. Constrained energy minimization allows the stress associated with the equilibrium process to be determined and a phenomenological relation allows the stress associated with dissipative process to be characterized. As part of the model predictions, the hysteresis loop associated with the pseudoelastic behavior comes naturally out of the loading–unloading process, with the energy required for both phase nucleation and interface propagation contributing to the dissipation.

The required input to the model include the elastic constitutive relations of the WZ and HX phases which are obtained from independent MD calculations for specific wire sizes and temperatures, values of the maximum interfacial energy $u_{\text{int}}^{\text{m}}$ and the maximum dissipative stress $\sigma_{\text{d}}^{\text{m}}$ which are obtained by fitting to MD results, and the values of certain critical strains (forward WZ$\rightarrow$HX nucleation strain ($\varepsilon_{\text{s}}^{\text{L}}$) and reverse HX$\rightarrow$WZ nucleation strain ($\varepsilon_{\text{s}}^{\text{U}}$)) which are also obtained from MD data.

The model is used to quantify the behavior of ZnO nanowires with lateral dimensions between 20 and 40 Å over the temperature range of 100–500 K. Excellent agreement with data from MD simulations is obtained. It is found that the size dependence of behavior arises primarily from the effect of surfaces on the strain energy or elastic constitutive relations of the WZ and HX phases and the relative importance of surface and bulk in determining the energy associated with the interface between the WZ and HX phases. This size effect is reflected in the model phenomenologically through lower phase equilibrium stress and lower interfacial energy at smaller wire sizes. The dependence of the overall pseudoelastic behavior on temperature comes primarily from the dissipative process of interface propagation. Specifically, the higher thermal energy levels at higher temperatures reduce the amount of mechanical work (therefore the stress) required to overcome the barriers for interface propagation. This effect is reflected in the model phenomenologically through lower values of the maximum dissipative stress at higher temperatures.

Acknowledgments

Support through NSF Grant no. CMS9984298 and NSFC Grant no. 10528205 is gratefully acknowledged. Computations are carried out at the NAVO, ARL and ASC MSRCs through AFOSR MURI No. D49620-02-1-0382.

References

Abeyratne, R., Bhattacharya, K., 2001. Strain–Energy Functions with Multiple Local Minima: Modeling Phase Transformations Using Finite Thermoelasticity. Cambridge University Press.

Abeyratne, R., Kim, S.-J., 1994. A one-dimensional continuum model for shape memory alloys. Int. J. Solids Struct. 31, 222–2249.

Abeyratne, R., Knowles, J.K., 1993. A continuum model of a thermoelastic solid capable of understanding phase transitions. J. Mech. Phys. Solids 51, 541–571.

Binks, D.J., Grimes, R.W., 1993. Incorporation of monovalent ions in ZnO and their influence on varistor degradation. J. Am. Ceram. Soc. 76 (9), 2370–2372.

Claeyssens, F., Freeman, C.L., et al., 2005. Growth of ZnO thin films—experiment and theory. J. Mater. Chem. 15, 139–148.

Fedelich, B., Zanzotto, G., 1992. Hysteresis in discrete systems of possibly interacting elements with a double-well energy. J. Nonlinear Sci. 2 (3), 319–342.

Freeman, C.L., Claeyssens, F., et al., 2006. Graphitic nanofilms as precursors to wurtzite films: theory. Phys. Rev. Lett. 96, 066102-1-4.

Gall, K., Lim, T.J., et al., 2000. Role of intergranular constraint on the stress-induced martensitic transformation in textured polycrystalline NiTi. Int. J. Plast. 16 (10), 1189.

Haile, J.M., 1997. Molecular Dynamics Simulation. Wiley-Interscience, New York.

Hirsinger, L., Creton, N., et al., 2004. Stress-Induced Phase Transformations in Ni–Mn–Ga Alloys: Experiments and Modelling. Elsevier, Cirencester, UK.

Huo, Y., Muller, I., 2003. Interfacial and inhomogeneity penalties in phase transitions. Continuum Mech. Thermodyn. 15 (4), 395.

Kulkarni, A.J., Zhou, M., 2006a. Size-dependent thermal conductivity of zinc oxide nanobelts. Appl. Phys. Lett. 88, 141921-1-3.
Kulkarni, A.J., Zhou, M., 2006b. Size-effects-dominated thermal and mechanical responses of zinc oxide nanobelts. Acta Mech. Sin. 22, 217–224.
Kulkarni, A.J., Zhou, M., et al., 2005. Orientation and size dependence of the elastic properties of ZnO nanobelts. Nanotechnology 16 (12), 2749–2756.
Kulkarni, A.J., Zhou, M., et al., 2006. Novel phase transformation in ZnO nanowires under tensile loading. Phys. Rev. Lett. 97, 105502-1-4.
Kulkarni, A.J., Sarasamak, K., et al., 2007. Characterization of novel pseudoelastic behavior of zinc oxide nanowires. Philos. Mag. 87 (14–15), 2117–2134.
Landman, U., Luedtke, W.D., et al., 1996. Reversible manipulations of room temperature mechanical and quantum transport properties in nanowire junctions. Phys. Rev. Lett. 77 (7), 1362.
Liang, W., Zhou, M., 2005. Pseudoelasticity of single crystalline Cu nanowires through reversible lattice reorientations. J. Eng. Mater. Technol. 127, 123–133.
Liang, W., Zhou, M., 2006. Atomistic simulations reveal shape memory of fcc metal nanowires. Phys. Rev. B (Condens. Matter) 73, 115409-1-11.
Liang, W., Zhou, M., et al., 2005. Shape memory effect in Cu nanowires. Nano Letters 5 (10), 2039–2043.
Liang, W., Srolovitz, D.J., et al., 2007. A micromechanical continuum model for the tensile behavior of shape memory metal nanowires. J. Mech. Phys. Solids 55, 1729–1761.
Melchionna, S., Ciccotti, G., et al., 1993. Hoover NPT dynamics for systems varying in shape and size. Mol. Phys. 78 (3), 533–544.
Muller, I., 1989. On the size of the hysteresis in pseudoelasticity. Continuum Mech. Thermodyn. 1 (2), 125.
Muller, C., Bruhns, O.T., 2006. A thermodynamic finite-strain model for pseudoelastic shape memory alloys. Int. J. Plast. 22 (9), 1658.
Muller, I., Xu, H., 1991. On the pseudo-elastic hysteresis. Acta Metall. Mater. 39 (3), 263.
Musolff, A., Sahota, H., 2004. Phase transitions in the shape memory alloy CuAlNi. Continuum Mech. Thermodyn. 16 (6), 539.
Park, H.S., Gall, K., et al., 2005. Shape memory and pseudoelasticity in metal nanowires. Phys. Rev. Lett. 95, 255504-1-4.
Raniecki, B., Lexcellent, C., 1994. R_L-models of pseudoelasticity and their specification for some shape memory solids. Eur. J. Mech., A—Solids 13 (1), 21.
Raniecki, B., Lexcellent, C., 1998. Thermodynamics of isotropic pseudoelasticity in shape memory alloys. Eur. J. Mech., A—Solids 17 (2), 185.
Sander, S., 2003. Surface stress: implications and measurements. Curr. Opin. Solid State Mater. Sci. 7, 51–57.
Spearot, D., Jacob, K., et al., 2005. Nucleation of dislocations from [0 0 1] bicrystal interfaces in aluminum. Acta Mater. 53 (13), 3579–3589.
Truskinovsky, L., Vainchtein, A., 2004. The origin of nucleation peak in transformational plasticity. J. Mech. Phys. Solids 52 (6), 1421.
Wang, Z.L., 2004a. Functional oxides nanobelts—materials, properties and potential applications in nanosystems and biotechnology. Annu. Rev. Phys. Chem. 55, 159–196.
Wang, Z.L., 2004b. Nanostructures of zinc oxide. Mater. Today, 26–33.
Wang, Z.L., 2004c. Zinc oxide nanostructures: growth, properties and applications. J. Phys.: Condens. Matter 16, R829–R858.
Wang, J., Kulkarni, A.J., et al., 2007a. Novel mechanical behavior of ZnO nanorods. Comput. Meth. Appl. Mech. Eng., doi:10.1016/j.cma.2007.10.011.
Wang, J., Kulkarni, A.J., et al., 2007b. Molecular dynamics and density functional studies of a body-centered-tetragonal polymorph of ZnO. Phys. Rev. B (Condens. Matter Mater. Phys.) 76, 172103-1-4.
Wolf, D., Keblinski, P., et al., 1999. Exact method for the simulation of Coulombic systems by spherically truncated, pairwise r^{-1} summation. J. Chem. Phys. 110 (7), 8254–8282.
Yakobson, B.I., Brabec, C.J., et al., 1996. Nanomechanics of carbon tubes: instabilities beyond linear response. Phys. Rev. Lett. 76 (14), 2511.